Planetary Defense Conference 2015
Frascati, ITALY

IAA-PDC-15-05-05

Wave Generation, Wave Propagation and Onshore Consequences of the 2015 PDC Asteroid-Impact Scenario

Souheil M. Ezzedine[(1)(2)], Paul L. Miller[(1)], David S. Dearborn[(1)]
[(1)]*Lawrence Livermore National Laboratory, PO Box 808, Livermore, CA, 94551*
[(2)] *Corresponding author;*

Keywords: *asteroid, impact, waves, simulation, hazards*

Abstract
A hypothetical asteroid-impact scenario will be used as the basis for discussion and analyses during the PDC 2015 table-top exercise. The asteroid is discovered on 13 April 2015, at magnitude 20.9, declination -39^{o}, and is classified as a potentially hazardous asteroid. The asteroid size is initially estimated between 100-500 meters. The large size uncertainty is due to uncertainties in both albedo and absolute-magnitude values. As the object is tracked over subsequent weeks, the probability of impact in September 2022 continues to rise, but the asteroid's impact-risk region is much longer than the diameter of the Earth, with a narrow width. The risk corridor wraps more than halfway around the globe from the Caspian Sea to the Pacific Ocean. Roughly two thirds of the corridor is over water while the other third is on land. Based on this script and because there is a high probability of water impact, we simulate water impacts at several locations along the risk corridor: in the South China Sea, the Sulu Sea, and the Pacific Ocean. We have simulated the problem from source (asteroid entry) to ocean impact (splash) to long wave generation, propagation, and interaction with the shoreline. The effects of the asteroid on the ocean surface are simulated using the hydrocode GEODYN to create the wave source for the shallow water wave propagation code, SWWP. The GEODYN-SWWP coupling is based on the structured adaptive mesh refinement infrastructure, SAMRAI, and has been used in FEMA table-top exercises conducted in 2013 and 2014. Results from the wave-propagation simulations can be used to estimate onshore effects or can inform more sophisticated inundation (flooding) models, not included in this discussion. We describe previous results of this methodology, including models of impacts off the East Coast of the United States, in the Gulf of Mexico, and near San Francisco. For the PDC 2015 exercise object, because the size of the asteroid is not deterministically known, we explore the effect of asteroid size on the landfall waves at several shoreline cities of interest near the potential impact area. We construct a probability of wave height given the size of the asteroid and the location of the impact along the risk corridor. Such probability profiles can inform emergency response and disaster-mitigation efforts, and may be used for design of maritime protection (e.g. jetties, breakwaters walls) or assessment of risk to shoreline structures of interest (e.g. bridges, power plants).

1. Brief description of GEODYN and SWWP

1.1. General guidelines for the preparation of your text

Following Lomov et al. [1, 2], simulations presented in this paper are conducted using GEODYN – a parallel Eulerian compressible solid and fluid dynamics code with AMR capabilities [3, 4]. Among its many features are high-order material interface reconstruction algorithms [5] and advanced constitutive models that incorporate salient features of the dynamic response of geologic media [6]. GEODYN is able to: a) simulate materials under extremely large deformations, b) resolve details of wave propagation within grains with high accuracy, and c) use a continuum damage mechanics approach to represent fracture. The Eulerian framework of adaptive mesh refinement [7] is a relatively mature technique. Adaptive mesh refinement can help simulating the entire domain while allowing focus on greater details in regions of interests. In combination, Eulerian Godunov methods with AMR have been proven to produce highly accurate and efficient solutions to shock capturing problems. The method used here is based on several modifications of the single-phase high-order Godunov method, which is not as straightforward as Lagrangian FEM. For completeness we will be briefly summarize the method. For solid mechanics, the governing equations consist of the laws of conservation of mass, momentum and energy, equation of distortional elastic deformation, and a number of equations that represent specific rheological time-history dependent parameters (i.e. porosity, plastic strain). The viscoplasticity is modeled with a measure of elastic deformation as a symmetric, invertible, positive definite tensor which is determined by integrating the correspondent evolution equation [8]. The numerical scheme for a single fluid cell is based on the approach of Miller [9], with some modifications to account for the full stress tensor associated with solids. The multidimensional equations are solved by using an operator splitting technique, in which the one-dimensional Riemann problems for each direction are solved using Strang-splitting order to keep second-order accuracy,

while the source term is always applied at the end of the time step. Each directional operator is the update of the cell from two-consecutive present-future time steps with fluxes computed at the edges of the cell. The approach to modeling multi-material cells is similar to that in Miller [9] but extensively improved in Lomov et al [1, 2].

1.2. The shallow water wave propagation code SWWP

It is often assumed that any source of disturbance, in particular tsunamis, propagates in the open ocean are linear, non-dispersive surface waves [10]. Therefore, the shallow water equations (SW) have often been used. Assumption of linearity of the waves stems from the fact that the ratio of water surface displacement to the depth is small. For non-dispersive waves, the propagation speed does not depend on their frequency. Dispersion alters wave speeds leading to waves with shorter wavelength to travel more slowly. In the long-wave limit (or hydrostatic approach), all waves travel with the same speed $C=(g\,H)^{1/2}$, where g is the acceleration of gravity, and H is the local water depth [10]. This wave speed relationship makes it relatively easy to estimate travel-time for a tsunami event. Tsunami modeling based on linear shallow water equations (LSW) can predict initial arrival times quite accurately, because the leading wave in a real wave train is the longest and propagates with the biggest wave speed. The models that include nonlinearity but still neglecting effects of frequency dispersion are governed by the nonlinear shallow water equations (NLSW). NLSW-based models can quite often provide good prediction of run-up heights of the leading wave [11]. The principal limitation of their accuracy in predicting shoreline inundation in tsunami application stems from factors that are not covered by the basic theory: a) frequency dispersion that can lead to different wave heights and wave forms, b) inability of wave breaking simulation due to singularity in the free surface description, c) interaction with fixed structures, and the interaction with the mass of transported debris resulting from destruction of structures. While effect of dispersion still can be included as an extension to SW equation, other effects mentioned above require more complicated approach [10, 11]. One of the most advanced examples of NLSW modeling is MOST (Method of Splitting Tsunami; [12]) used at National Oceanic and Atmospheric Administration (NOAA). A number of applications of this model to different tsunami scenarios are described in the literature (e.g. [13, 14]). Another model that uses NLSW using Godunov method and Adaptive Mesh Refinement technique was proposed by LeVeque [15]. SWWP is essentially a Godunov NLSW implementation using LLNL's SAMRAI (Structured Adaptive Mesh Refinement Application Infrastructure [16]).

2. Water wave source generation using GEODYN

LLNL's team has participated in two tabletop exercises conducted at the FEMA headquarters in 2013 (TTX1) and 2014 (TTX2). We have set up GEODYN to simulate the source wave at the impact sites. The size of the assumed spherical asteroid is 50m in diameter. Impact locations are 100km off the Maryland coast for TTX1 and 100km off the Louisiana coast for TTX2. The density of the asteroid is assumed to be ~8 and ~2.2 g/cm^3 for TTX1 and TTX2, respectively while the impact velocity is ~13km/s and ~15 km/s for TTX1 and TTX2, respectively. The entry angle is set to 20^o for TTX1 while 39^o for TTX2. Each 3D simulation required approximately 9 million cells, and 4 levels of AMR and a total of ~10,000 CPU-hours and nearly 32TB of storage space on LLNL's HPC resources. For illustration purposes we have depicted four time-history snapshots of the impact of the asteroid on the ocean surface. We would like to re-emphasizes that the simulation has been conducted in three-dimensional space and that the computational domain include not only the ocean but also the atmosphere.

Figure 1 depicts vertical cross-section of four frames. First frame shows the entry trajectory and initial impact; air (green) and ocean (red) as well as the phase transition of water into vapor (blue). Last frame shows the development of water rims and ejecta as well the complexity of the physical processes that take place including the breakup of the rim and the collapse of the wave. Ocean base (no shown here) was assumed to be basalt. It is worth noting that the ring of compressed water around the impact site, while the phase changes take places at the shoulder of the "crater" and at the bottom end of the impact which is in good agreement with several observations in real tests conducted at the Nevada Test and the Pacific Ground Test. Time-history of the height of the water wave at the source were recorded around the impact location, 300m away from the source at 36 azimuthal directions (one marker point every 10^o). These time-histories are then passed directly to SWWP for wave propagation at long distances until their interceptions to the shorelines.

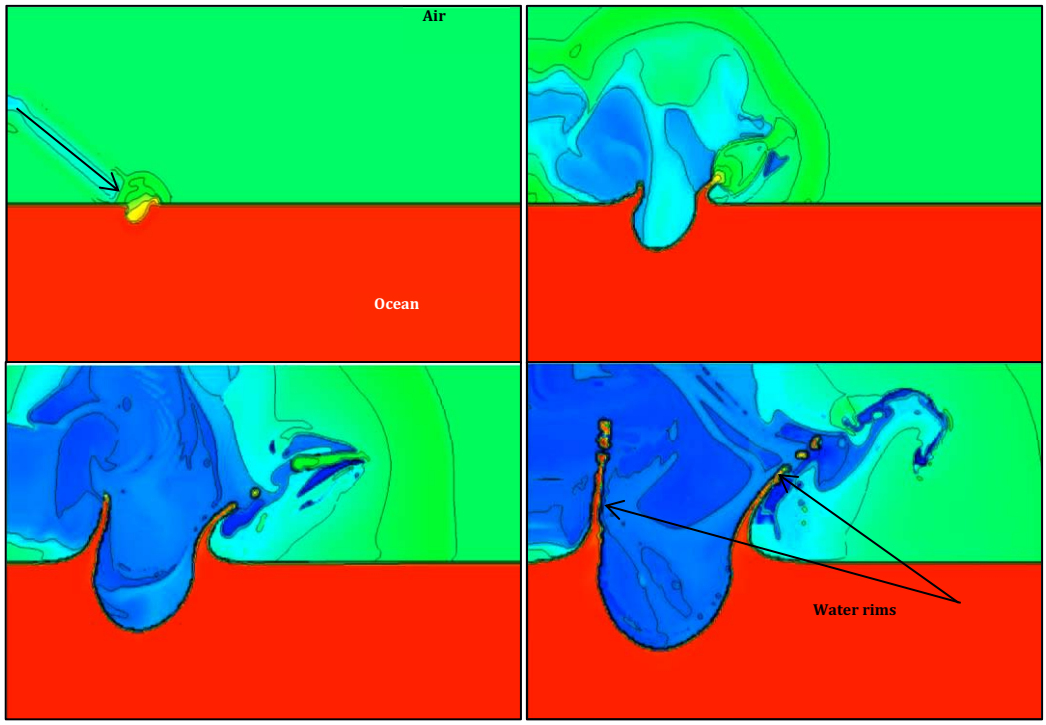

Figure 1: Time snapshots of the impact of an asteroid on ocean surface. First frame shows entry trajectory and initial impact. Simulation includes air (green) and ocean (red) as well as the phase transition between of water into vapor (blue). Last frame shows the development of water rims and ejecta as well the complexity of the physical processes.

3. Water wave propagation using SWWP

In the present section we will illustrate the application of GEODYN-WPP coupling to TTX1 and TTX2. As a reminder the first site is located off the shorelines of Maryland.TTX1 was designed for the first table-top exercise (TTX1) conducted in 2013. The site is characterized by open seas and the trajectory of the impactor is away from the shorelines (divergent waves). The second site for TTX2 is located in the Gulf of Mexico where the impactor characteristics and its trajectory are totally different from the former scenarios. TTX2 conducted in 2014 featured four different impact site locations and the waves are mainly contained within the Gulf (entrapped waves). Figure 2 depicts results from both tabletop exercises.

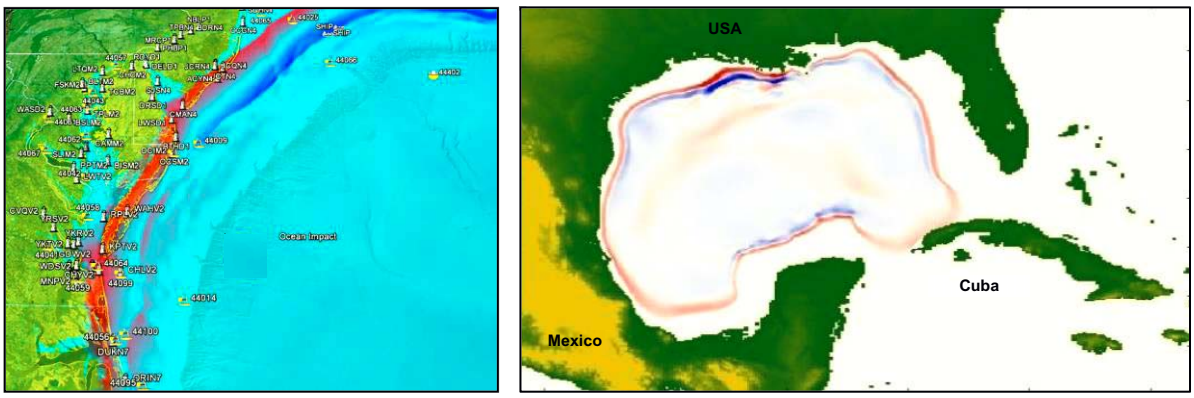

Figure 2: Example of application of LLNL's integrated tool for two tabletop exercises. Left frame show a water wave simulation to the east coast shore of the USA due to a 50m diameter asteroid impact at 100km of off the Maryland shorelines while the right frame depicts the impact of a similar asteroid in the Gulf of Mexico of the Louisiana shorelines. Both snapshots are taken at ~2 hours from impact.

Subsequent hazard analyses were conducted by LLNL for TTX1 and included several sectors such as a) maritime and navigation, b) surface transportation, c) law and enforcement agencies, d) emergency facilities and agencies, e) military and coast guards and f) telecommunications for TTX1 are shown on Figure 3. Hazards analyses for TTX2 were conducted by Sandia National Laboratories (SNL) and they are not shown here.

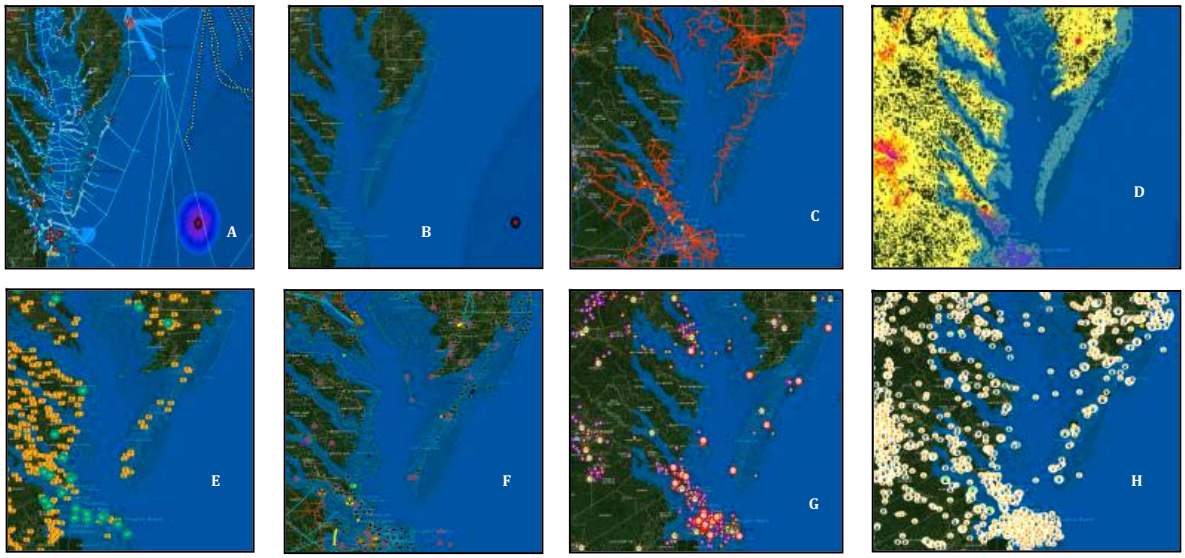

Figure 3: Example of consequences of Tsunami on the shoreline of US coast due to asteroid impact on the Atlantic ocean off the Maryland coast -- TTX1 (2013). A: Maritime navigation – general paralysis of the navigation system; B: Flood 3Hr post impact – elephant truck region totally flooded; C: Transportation – severe disturbance of evacuation arteries; D: Normal daytime population – evacuation of large population; E: Enforcement agencies – prisons & police stations are impacted; F: Emergency facilities – hospitals, shelters, EMS & fire stations; G: Military, US Coast guard – evacuation/recovery affected; H: Telecommunications – emergency announcement disturbed.

4. Simulation of 2015 IAA Planetary Defense Conference (PDC) tabletop exercise

4.1. PDC hypothetical asteroid impact scenario

The 2015 PDC hypothetical asteroid impact scenario has been constructed (scripted) by Chodas [http://neo.jpl.nasa.gov/pdc15/]. It is reproduced here for completeness. At the 2015 IAA Planetary Defense Conference (PDC), held April 13 - 17, 2015 in Frascati, Italy, a hypothetical asteroid impact scenario was presented and used as a basis for discussion. Although this scenario is realistic in many ways, it is completely fictional and does not describe a real potential asteroid impact. The scenario unravels (unveil) as follows:

- The asteroid is discovered on April 13, 2015, the first day of the conference, at magnitude 20.9, declination -39 degrees and heading south. It is assigned the designation "2015 PDC" by the Minor Planet Center, and classified as a Potentially Hazardous Asteroid (PHA) based on its orbit.
- The asteroid's orbital elements are known fairly accurately even in the first few days. Its mean distance from the Sun (semi-major axis) is 1.77 au, and the orbital eccentricity is 0.49. Its perihelion distance is 0.90 au and aphelion distance is 2.65 au; the orbital period is 864 days (2.37 years). The orbital inclination is fairly small: 5.35 deg. The asteroid's orbit comes very close to the Earth's orbit on its outbound leg, much like the Chelyabinsk impactor, however unlike Chelyabinsk, the current asteroid impacts at its ascending node.
- Very little is known about the object's physical properties. Its absolute magnitude is estimated to be about H = 21.3 +/- 0.4, which puts the asteroid's size at roughly 100 to 500 meters. The large size uncertainty is due to uncertainties in both albedo and magnitude value.
- At discovery, the asteroid is quite distant from the Earth, about 0.34 au (51 million kilometers or 32 million miles). It is approaching our planet and slowly brightening, but it peaks at only magnitude 20.3 on May 4. It reaches a closest approach of about 0.19 au (28 million km or 18 million miles) from Earth on May 12. It never gets within range of the Goldstone radar and it's too far south at close approach for the Arecibo radar.
- The JPL Sentry system and University of Pisa's CLOMON system both identify many potential impacts for this object at several future dates. The most likely potential impact date is 2022 Sep 3, but the impact probability for that date is still low in the first week after the asteroid is discovered. Nevertheless, as the object is tracked over the next few weeks, the impact probability for 2022 starts to climb, reaching 0.2% a month after discovery. Even as the asteroid fades past magnitude 22 in early June, it continues to be observed and tracked since the chance of impact just keeps rising.
- The first part of the scenario ends in mid-June 2015, when the probability of Earth impact in 2022 has reached 1% and continues to rise. The rest of the scenario will be played out at the conference.
- It is clear that the object will be observable through the rest of 2015, although it will be quite faint (22nd and 23rd magnitude) and observers will require fairly large (2-meter-class) telescopes to track it.

In December 2015 and January 2016, the asteroid will fade through 24th and 25th magnitudes, requiring very large aperture telescopes such as the 4- and 8-meter class facilities of CFHT, Keck, Gemini, Subaru, VLT, etc. In the spring of 2016, the asteroid will move too close to the Sun to observed, and it will remain unobservable for about 7 months.

- The asteroid's uncertainty region at the time of the potential impact is much longer than the diameter of the Earth, but its width is much less. The intersection of the uncertainty region with the Earth creates the so-called risk corridor across the surface of the Earth. The corridor wraps more than halfway around the globe, as depicted by the red dots on Figure 4.

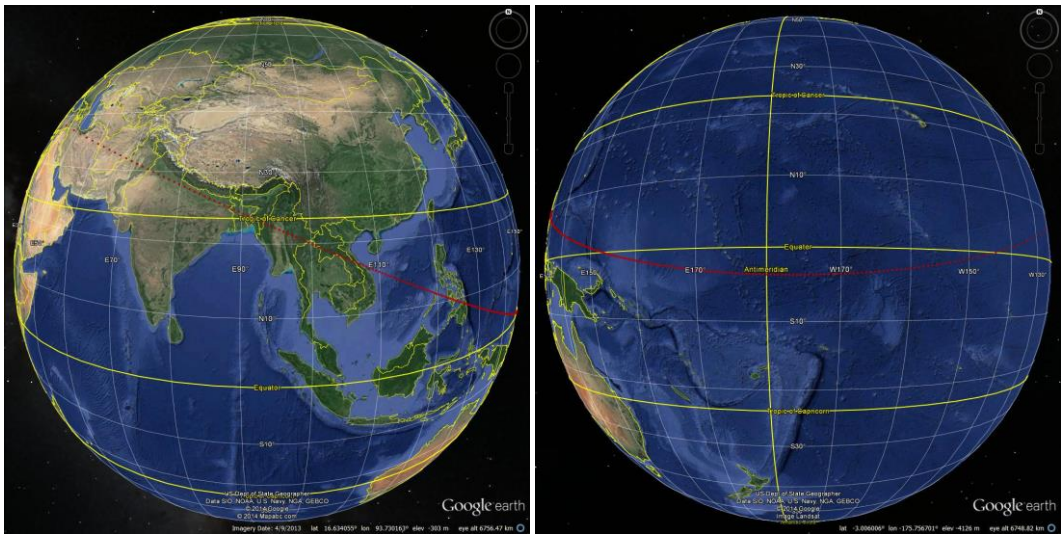

Figure 4: PDC 2015 tabletop exercise (TTX) as scripted by Chodas [http://neo.jpl.nasa.gov/pdc15/]. The risk corridor spans Turkey through India through south-east Asia through the Pacific Ocean; almost half of the globe. Red dots depict the possible sites of impacts.

4.2. Three postulated scenarios

Due to the uncertainty in the size of the asteroid and it impact location we have defined three different impact scenarios for demonstration and simulation purposes and they are given as follows:

1. The first impacted scenario postulate an asteroid of 400m diameter impacting site #1 as depicted on Figure 5a. The asteroid has a density of 2.2 g/cm^3, 4^o angle of attack and a velocity of 15.3 km/s.
2. The second impact site is #151 (Figure 5b) of the risk corridor and the asteroid has the same size and density as in the first scenario whoever the angle of attack is set to 72^o and a velocity of 15.7 km/s.

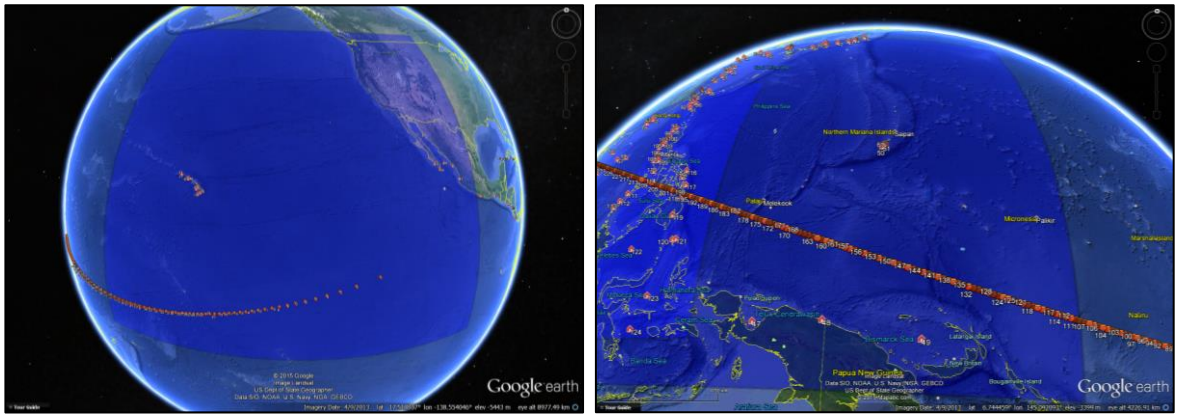

Figure 5: PDC 2015 TTX1 (left) & TTX2 (right): this google-earth image depicts the computational domain (patch) the risk corridor of the asteroid (dark red dots) and the location of the gauge station (red shed).

3. The third scenario calls for an asteroid of 100m diameter impacting site #229 (Figure 6) with an angle of attack of 54^o and a velocity of almost 16 km/s. Even though we have conducted the simulation with 100m diameter we will present here a deviation from this scenario using an asteroid of 50m diameter. This latter scenario has been adopted prior to the PDC TTX 2015 public release of the final script.

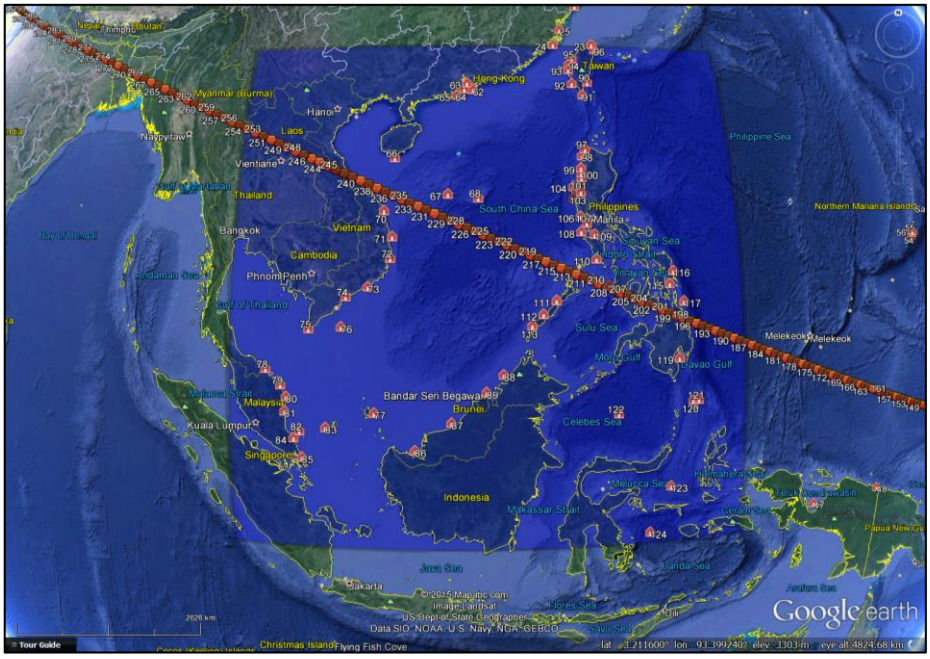

Figure 6: PDC 2015 TTX3: this google-earth image depicts the computational domain (patch) the risk corridor of the asteroid (dark red dots) and the location of the gauge station (red shed). The computational domain covers South China Sea and its neighboring countries.

4.3. Simulation of PDC 2015 TTX scenario #1

Figure 7 depicts twelve snapshots of the numerical simulation of ocean wave generation and propagation due to asteroid impact at site #1 of the risk corridor established by Chodas [http://neo.jpl.nasa.gov/pdc15/]. Time flows from left to right and top to bottom. One can locate the Hawaiian Islands and the coasts of Mexico and California. The 12 snapshots represent 3 hours history from the time of impact. Waves reach Baja California, Ecuador and Peru within 2 hours from impact. The height of the waves reach +/- 5m and get attenuated as they travel north reaching as far as the west coast of the USA and Alaska. The impact is taken place in a deep open ocean; initially three long wave crests are developed for 2 hours. After two hours only one main long wave sustains the course of time.

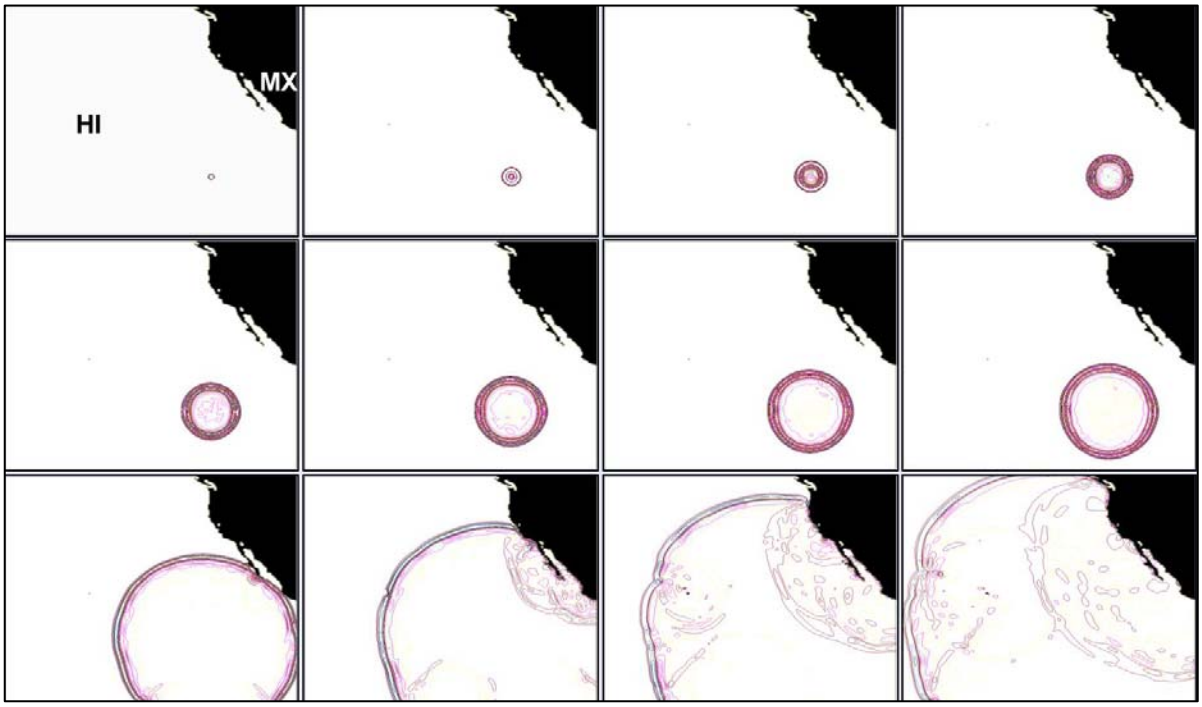

Figure 7: PDC 2015 TTX1: twelve snapshots of the numerical simulation of the ocean waves generation and propagation due to asteroid impact. Time flows from left to right and top to bottom.

4.4. Simulation of PDC 2015 TTX scenario #2

Figure 8 depicts eight snapshots of the numerical simulation of ocean wave generation and propagation due to asteroid impact at site #151 of the risk corridor. The impact location is off of the coast of Papua and New-Guinea. Eight snapshots total 2 hours history from the time of impact. Waves reach of Papua/New-Guinea within 1 hour from impact. The height of the waves reach +/- 7m and attenuate with time. The impact is taken place in shallower ocean compared to the previous scenario; again initially three long wave crests are developed within 45 minutes but only two main long wave sustains the course of time and reaches as far as the Philippines, Japan and China among other south-east Asian countries as shown on Figure 9.

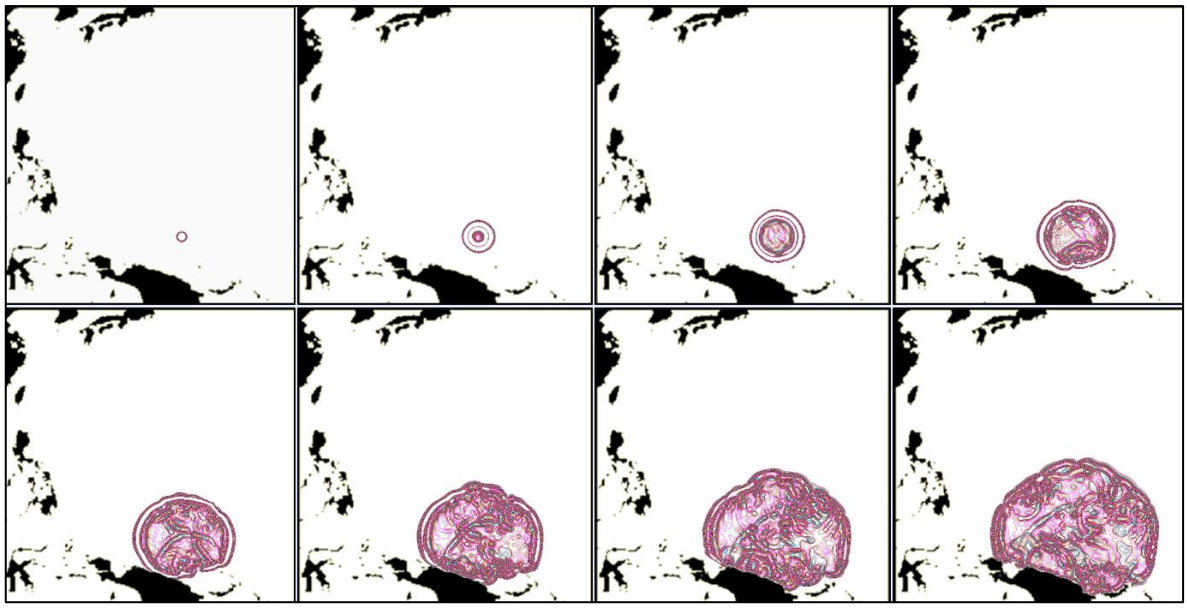

Figure 8: PDC 2015 TTX2: eight snapshots of the numerical simulation of the ocean waves generation and propagation due to asteroid impact. Time flows from left to right and top to bottom. The impact location is site #151 on the risk corridor.

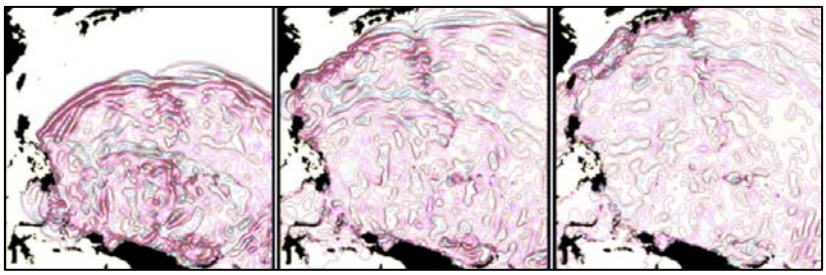

Figure 9: PDC 2015 TTX2: three later time of the numerical simulation of the ocean waves generation and propagation. One can notice a "wall" of water reaching several countries such as the Philippines, Japan, and China among others.

4.5. Simulation of PDC 2015 TTX scenario #3

Figure 10 depicts eight snapshots of the numerical simulation of ocean wave generation and propagation due to asteroid impact at site #229 of the risk corridor. The impact location is within South China Sea. The eight snapshots represent 2 hours history from the time of impact. Waves reach Vietnam then south of China within 1 hour from impact. The height of the waves reach +/- 2m. The impact is taken place in "enclosed" ocean compared to the two previous scenarios. The ocean is little shallower than in scenario #1 but deeper than that of #2; initially only two long wave crests are developed within 30 minutes but only one main long wave sustains the course of time and reaches the Philippines, China and Taiwan among other south-east Asian countries.

It worth noting the richness of the water wave field in the last two impact scenarios; this is mainly due to the bathymetry of the ocean. In fact Southeast Asia is a quilt of continental fragments, seamounts and terranes and intra-oceanic island arcs that were welded to the Asian continent due to tectonic activities leading to the creation of several trenches and depression within the region. Due to earthquakes activities, the region is well known for the genesis of the most devastating tsunamis in the world.

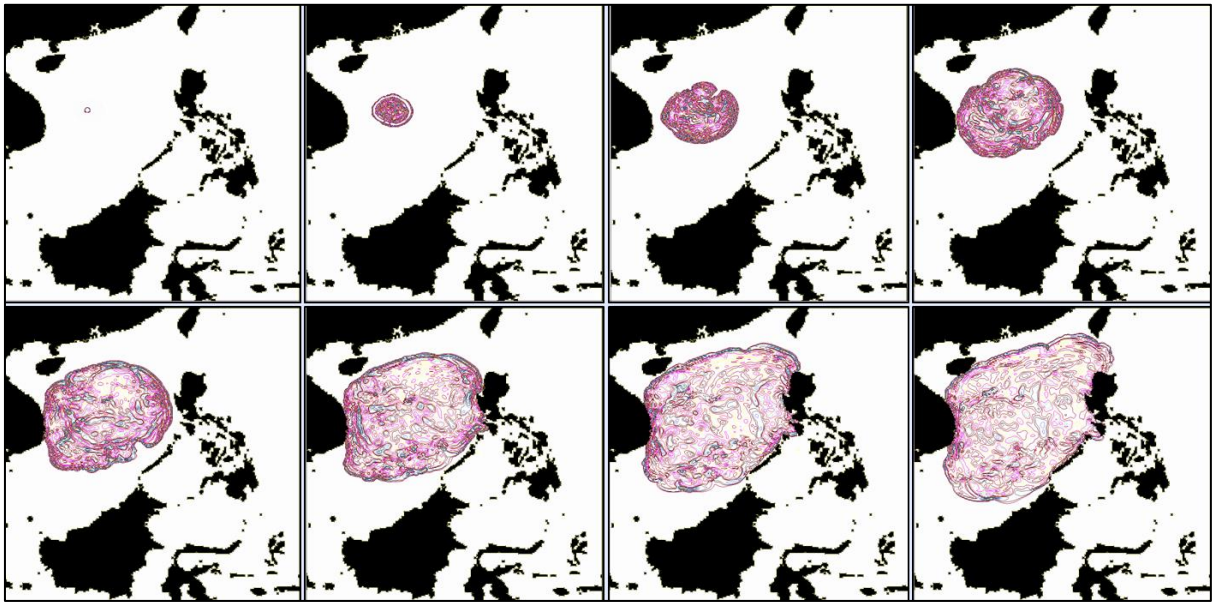

Figure 10: PDC 2015 TTX2 Three views of the simulation of the source of the water waves at 3.211 milliseconds calculated using GEODYN. Air (bleu) and ocean (red) are shown; a basaltic ocean floor is not shown here. Countries include: Vietnam, Chinese coast (Hong-Kong) , Taiwan, Malaysia, Brunei and of course several on the coast of Philippines – islands: Paracel, Spratly, Riau and the Palawan keys which act as a levee for the Sulu sea and the majority of the islands of the Philippines.

5. Toward a probabilistic risk profiles of water wave heights

Because of the uncertainty associates with the impact risk corridor we proceeded to assess the effect of the hypothetical impact locations on the water wave reaching the shores of coastal cities. The resulting heights of waves reaching coastal cities of interest have been reduced to maximum- and minimum-envelopes-of-water profiles. Using such data enables a range of expected inundation risk profiles and inundation maps for each impact. It should be noted that the impact locations were idealized and binned -- based on impact velocity, angle of attack and ocean depth -- into a few GEODYN source simulations due to the HPC-CPU requirements for each simulation. There are as many as 40 cases that have been simulated along the impact risk corridor. Results of the top ten simulation results are shown on Figure 11 for two cities located on the coast of Vietnam and China, respectively. Figure 11 depicts the maximum water level forecast at both cities for all 10 simulations and as many as 4 impact bins for the source generation. The minimum (thick green line) and maximum (thick red line) water level heights are also plotted on Figure 11 and could be used directly into an inundation model to produce maps of flooding for risk assessment, emergency preparedness and evacuation planning. It is worth noting that the combination of all the simulations could be done in a probabilistic framework, however the probability of impact at each location is not available and this procedure is beyond the scope of the present study; we will present the framework in a future study.

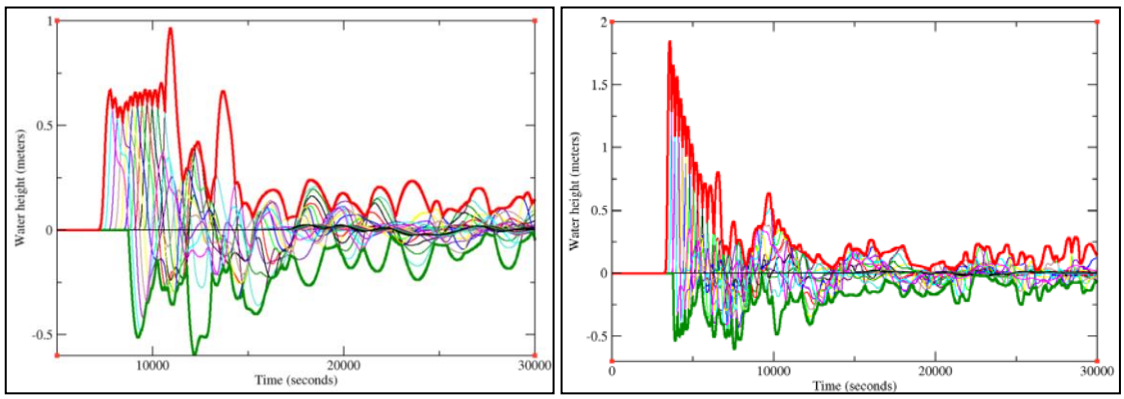

Figure 11: wave height profiles for two cities located in the South China Sea. Each curve is obtained by running several numerical simulation of the asteroid impact at several locations within the PDC 2015 TTX computational domain. The overall upper (thick red) and lower (thick green) wave height envelops are also depicted.

6. Summary/Conclusions

We have uniquely established a numerical coupling between the hydrocode GEODYN and the shallow water wave program SWWP to address impacts of asteroid on surface oceans, the subsequent long water wave generation and their interception with the shorelines. The GEODYN-SWWP has been exercised for the second FEMA-NASA asteroid-impact table top exercise (TTX2) held at FEMA HQ on 20 May 2014, while an early version using similar approach to [19] has been used in TTX1. The current approach, using GEODYN-SWWP, offers unique capabilities to address the full scale interactions of asteroids with the ocean (source) and the interactions of the water waves with the shorelines and maritime structures for consequence analyses. We have applied this unique capability to 2015 PDC hypothetical asteroid impact scenario. We have simulated three main scenarios at three different impact locations; two of them are located in the Pacific Ocean while the third in the South China Sea. Results of the resulting wave propagation have been presented and maximum- and minimum-envelopes-of-water at several coastal cities have been established and could be used directly into an inundation model to produce maps of flooding for risk assessment, emergency preparedness and evacuation planning. This approach has been conducted into a deterministic framework and would be extended into a probabilistic one in the future.

7. Acknowledgements

This work was partially funded by the NASA Near-Earth Object Program, and was performed under the auspices of the U.S. Department of Energy by Lawrence Livermore National Laboratory under Contract DE-AC52-07NA27344. We would like to thank Paul Chodas for NASA for sharing the TTX2 and the PDC 2015 TTX exercises and Mark Boslough and Barbara Jennings from Sandia National Labs for several discussions on TTX1, TTX2 and the PDC 2015 TTX. Partial support for the work was provided by the Near Earth Object Program Office at NASA HQ. LLNL-PROC-669200-DRAFT.

8. References

- [0] Chodas (2014) http://neo.jpl.nasa.gov/pdc15/, accessed on 5 Dec 2014.
- [1] Lomov I., E. Herbold, T. Antoun, P. Miller, 2013, Influence of Mechanical Properties Relevant to Standoff Deflection of Hazardous Asteroids, Procedia Engineering 58, 251 – 259, The 12th HVIS, 2013.
- [2] Vorobiev Yu O, B. T. Liu, I. N. Lomov, and T. H. Antoun, 2007. Simulation of penetration into porous geologic media. International Journal Of Impact Engineering, 34(4):721-731, Apr 2007.
- [3] Antoun T., I. Lomov, L. Glenn, 2001, Development and application of a strength and damage model for rock under dynamic loading, in: D. Elsworth, J. Tinucci, K. Heasley (Eds.), Proceedings of the 38th U.S. Rock Mechanics Symposium, Rock Mechanics in the National Interest, Balkema Publishers, pp369–374.
- [4] Lomov I., M. Rubin, 2003, Numerical simulation of damage using an elastic-viscoplastic model with directional tensile failure, Journal De Physique IV 110: 281–286.
- [5] Hertel E., R. Bell, 1992, An improved material interface reconstruction algorithm for Eulerian codes, Sandia National Laboratory report.
- [6] Rubin M.B., I. Lomov, 2003, A thermodynamically consistent large deformation elastic-viscoplastic model with directional tensile failure, International Journal of Solids and Structures 40 (17) 4299 – 4318.
- [7] Berger M.J., P. Colella, 1989, Local adaptive mesh refinement for shock hydrodynamics, Journal of Computational Physics 82 (1) 64–84.
- [8] Rubin M.B., O. Vorobiev, L. Glenn, 2000, Mechanical and numerical modeling of a porous elastic-viscoplastic material with tensile failure, International Journal of Solids and Structures 37 (13) 1841–1871.
- [9] Miller G. H., E. G. Puckett, 1996, A high-order godunov method for multiple condensed phases, Journal of Computational Physics 128 (1) 134–164.
- [10] Stoker J.J., 1992. Water Waves: The Mathematical Theory with Applications, Wiley International, 600pages.
- [11] Liu Philip L. F and Harry Yeh, 2008, Advanced Numerical Models For Simulating Tsunami Waves and Runup. 334 pages, Publisher: World Scientific Publishing Company
- [12] Titov, V. V. and C. S. Synolakis, 1998, Numerical modeling of tidal wave runup. Journal of Water, Port Coastal Eng., 124(4), 157-171.
- [13] Tang, L., V. V. Titov and C. D. Chamberlin. 2009. Development, testing, and application of site-specific tsunami inundation models for real-time forecasting. Journal of Geophysical Research, 114(C12), 1-22.

- [14] Gonzalez, F. I., E. L. Geist, B. Jaffe, U. Kanoglu, H. Mofjeld, C. E. Synolakis, V. V. Titov, D. Arcas, D. Bellomo, D. Carlton, T. Horing, J. Johnson, J. Newman, T. Parsons, R. Peters, C. Peterson, G. Priest, A. Veturanto, J. Weber, F. Wong, A. Yalciner. 2009. Probabilistic tsunami hazard assessment at Seaside, Oregon, for near- and far-field seismic sources. Journal of Geophysical Research, 114, 1-19.
- [15] LeVeque, R., George D. L., Berger M., 2011. Tsunami modeling with adaptively refined finite volume methods. Acta Numerica, 20 (2011), 211-289. Arieh Iserles, eds.
- [16] Gunney, B. T. N., A. M. Wissink, and D. A. Hysom, 2006, Parallel Clustering Algorithms for Structured AMR, Journal of Parallel and Distributed Computing, 66(11):1419-1430.
- [17] CEC, California Energy Commission 2012; The impacts of sea level rise on the San Francisco Bay, prepared by the Pacific Institute for the CEC, 32 pages, CEC-500-2012-014.
- [18] Chodas P., 2014, NEO threat tabletop exercise #2 (TTX2), May 20-21, 2014, proposed scenarios; 4/3/14.
- [19] Ward, S.N., 2010, Tsunamis, Encyclopedia of Physical Science and Technology, 18 pages. Springer NY, USA.